Basic Research in Cardiology (2020) 115:57
https://doi.org/10.1007/s00395-020-0817-z

ORIGINAL CONTRIBUTION

NAD^+ administration decreases microvascular damage following cardiac ischemia/reperfusion by restoring autophagic flux

You-Jun Zhang[1,2] · Mingchao Zhang[3] · Xiaona Zhao[1,2] · Kailei Shi[1,2] · Maoqing Ye[1,2] · Jiawen Tian[1,2] · Shaofeng Guan[1,2] · Weihai Ying[3] · Xinkai Qu[1,2]

Received: 13 February 2020 / Accepted: 27 July 2020 / Published online: 10 August 2020

Abstract

Microvascular damage is a key pathological change in myocardial ischemia/reperfusion (I/R) injury. Using a rat model of myocardial I/R, our current study has provided the first evidence that nicotinamide adenine dinucleotide (NAD^+) administration can significantly attenuate myocardial I/R-induced microvascular damage, including reduced regional blood perfusion, decreased microvessel density and integrity, and coronary microvascular endothelial cells (CMECs) injury. In studies with primary cultured CMECs under hypoxia/reoxygenation (HR) and a rat model of I/R, our results suggested that the protective effect of NAD^+ on CMECs exposed to HR or I/R is at least partially mediated by the NAD^+-induced restoration of autophagic flux, especially lysosomal autophagy: NAD^+ treatment markedly induced transcription factor EB (TFEB) activation and attenuated lysosomal dysfunction in the I/R or HR-exposed cells. Collectively, our study has provided the first in vivo and in vitro evidence that NAD^+ significantly rescued the impaired autophagic flux and cell apoptosis that was induced by I/R in rat CMECs, which is mediated in part through the action of TFEB-mediated lysosomal autophagy.

Keywords NAD^+ · Myocardial ischemia · Autophagic flux · Microvascular damage · Lysosomes

Introduction

Despite prompt restoration of epicardial coronary flow after myocardial infarction, normalization of flow at the myocardial or microcirculatory level is not always assured. Estimates of the percent of patients who achieve normal epicardial flow but have some sign of suboptimal microcirculatory perfusion, which has been widely considered an independent risk factor for worse clinical outcomes, is up to 56.9% [6]. Thus, the reduction of microvascular damage is an important target for adjunctive treatment in addition to reperfusion [17, 18]. However, many approaches fail to be effective when translated into clinical research [16, 17]. Therefore, strategies to reduce coronary microvascular damage and final infarct size need to be further developed.

Mechanisms underlying microvascular damage are multiple and interacting during myocardial ischemia/reperfusion (I/R), including coronary microvascular endothelial cells (CMECs) swelling, alteration of the vasoregulation, platelet activation, thrombosis formation, inflammatory cell adhesion, endothelial barrier disruption, and external compression of capillaries due to regional edema [5, 13]. Whereas the quantitative contribution of the different mechanisms to coronary microvascular damage and infarction is not clear, a role for CMECs death is decisive in all of them. Thus, regulating the mode of endothelial cell death may present specific targets for pharmacological cardioprotection.

Autophagic flux has been proposed as a pivotal mechanism of cell death in myocardial I/R injury [10, 24]. It is a process whereby degradation of damaged organelles and proteins to ensure cellular homeostasis and survival [27, 35]. Autophagic flux is including the induction and formation of autophagosomes and lysosomal autophagy, the latter of which consists of autophagosomes fusing and degrading by

✉ Weihai Ying
13052218008@163.com

✉ Xinkai Qu
quxk805@163.com

1 Department of Cardiology, Huadong Hospital, Fudan University, 221 West Yanan Road, Shanghai 200040, China

2 Shanghai Key Laboratory of Clinical Geriatric Medicine, Shanghai 200040, China

3 Med-X Research Institute and School of Biomedical Engineering, Shanghai Jiao Tong University, 1954 Huashan Road, Shanghai 200030, China

lysosomes. The induction of autophagosomes is reflected by increases in the abundance of key autophagic proteins light chain 3B (LC3B) and p62. With the progress of autophagy, the autophagic proteins per se will be degraded in lysosomes and thus their abundance decreased. The cardioprotection role of the early stage of autophagic flux in I/R injury has been extensively studied [9, 20, 23], however, there is no evidence showing that lysosomal autophagy (the late stage of autophagic flux) is involved in the pathogenesis of I/R-related endothelial injury. Recent studies have indicated that enhanced lysosomal autophagy positively regulates post-ischemic angiogenesis [7], and impaired lysosomal autophagy leads to endothelial autophagic apoptosis [39]. These results imply that lysosomal autophagy plays a pivotal role in the endothelial cell fate. Thus, development of alternative agents that ensure optimal regulation of lysosomal autophagy may provide a new promising therapy for I/R-related endothelial injury.

Nicotinamide adenine dinucleotide (NAD^+), also known as coenzyme I, has been shown involved in human umbilical vein endothelial cell senescence and cancer cell death by promoting lysosomal autophagy [12, 34, 38]. On the other hand, NAD^+ has been suggested to profoundly alleviate the myocardial I/R injury by mimicking ischemic preconditioning in human heart [37], as well as stimulating glycolysis [30], attenuating oxidative stress, improving mitochondrial function [19], and reducing apoptosis [41] in mouse or rat hearts. However, whether NAD^+ could alleviate the microvascular I/R injury through regulation of lysosomal autophagy was unclear. The aim of this study was, therefore, to investigate the role and potential mechanism of NAD^+ in I/R related microvascular damage.

Materials and methods

All of the chemicals were purchased from Sigma (St. Louis, MO, USA), except where specified. All studies were performed following recently published guidelines [2, 25].

Ethics statement

Animal studies were performed in accordance with the Guide for the Care and Use of Laboratory Animals of the National Institutes of Health and were approved by the Institutional Animal Care and Use Committee of the School of Biomedical Engineering, Shanghai Jiao Tong University (Permit Number: 2014001). All surgical procedures were performed under sodium pentobarbital anesthesia (30 mg/kg), in which all efforts were made to relieve animal suffering.

Myocardial ischemia and reperfusion

Male Sprague–Dawley rats (230–270 g) were provided by the SLRC Laboratory (Shanghai, China). An animal ventilator was used. Saline, NAD^+ (20 mg/kg, 100 mM) or chloroquine (CQ, 10 mg/kg, 100 mM) was injected intravenously right before ischemia or reperfusion, respectively. The left anterior descending branch was occluded by ligation after a left thoracotomy. After 90 min of ischemia, the ligation was loosened. The sham control rats were subjected to all same surgical procedure except ligation. Rats were sacrificed 24 h after reperfusion, respectively.

Determination of myocardial no-reflow areas and infarct size

Hearts were harvested after 24 h of reperfusion. Rats received a 2% solution of the perfusion marker thioflavin-S (1 ml/kg) through the veins. After 15 min, the rats were euthanized and the hearts excised. The heart was sliced into 1-mm thick transections. Thioflavin-S distribution was visualized and photographed by ultraviolet transmission light ($k = 365$ nm). Under ultraviolet transmission light, the thioflavin positive areas were green and light blue stained areas, and the thioflavin negative areas were tawny stained areas. The no-reflow area (i.e. thioflavin negative areas) was measured and analyzed using ImageJ (NIH, Bethesda, MD, USA). As for infarct size, hearts were harvested 24 h after reperfusion and washed three times with saline. The heart was also sliced into 1-mm thick transections, then incubated in 1% 2, 3, 5-triphenyltetrazolium chloride (TTC) for 20 min at 37 °C. Subsequently, all transections were photographed, and the infarct size was measured using Image J.

Isolation of primary rat CMECs

Primary CMECs cultures were prepared as described. Hearts were removed from 20-day-old Sprague–Dawley rats, the atria and great vessels were trimmed off, and tissue was finely minced followed by sequential digestion with 0.5 mg/ml collagenase and 0.25% trypsin (Thermo Scientific, Waltham, MA, USA). CMECs were separated from fibroblasts by differential plating and were transferred in gelatin coated cell culture flasks in media containing endothelial cell medium (Science Cell, Carlsbad, CA, USA), 10% fetal calf serum, 100 mol/l penicillin, streptomycin and heparin. When expanded CMECs reached 90% confluence, they were passaged. CMECs cultured within 3–5 passages were used for this study.

Hypoxia/reoxygenation (HR) modeling in vitro and cell treatments

CMECs were subjected to hypoxia in vitro for 6 h by replacing the culture medium with 'ischemia buffer' [137 mM NaCl, 5 mM HEPES, 1.5 mM $MgCl_2$-$2H_2O$, 4 mM KCl, 1.5 mM $CaCl_2$, and 20 mM Na-lactate (pH 6.2)] and incubating it in a three-gas incubator (Thermo Scientific) filled with 95% N_2 and 5% CO_2 to reduce the oxygen concentration to 1%. Reoxygenation treatment, which followed hypoxia and lasted for 18 h, was accomplished by replacing the 'ischemia buffer' with complete culture medium and incubating it under normoxic conditions. All indicated agents were administrated right before hypoxia. CMECs were treated with HR and indicated drugs as shown in results, respectively.

Assessment of cell viability

Cell death was determined with a flow cytometry based Annexin V/7-amino-actinomycin D (7-AAD) assay and intracellular lactate dehydrogenase (LDH) tests. The flow cytometry based Annexin V/7-AAD assay was performed using an ApoScreen Annexin V kit (Southern Biotech, Birmingham, AL, USA) according to the manufacturer's instructions. For the intracellular LDH assay, cell survival was quantified by measuring the intracellular LDH activity of the cells. Cells were lysed for 15 min in lysis buffer containing 0.04% Triton X-100, 2 mM HEPES and 0.01% bull serum albumin (pH 7.5). Then, 50 µl of cell lysate was mixed with 150 µl of 500 mM potassium phosphate buffer (pH 7.5) containing 0.34 mM NADH and 2.5 mM sodium pyruvate. The A340 nm changes were monitored over 90 s. The percentage of cell survival was calculated by normalizing the LDH values of samples to LDH activity measured in the lysates of control (wash only) culture wells. A terminal-deoxynucleoitidyl transferase mediated nick end labeling (TUNEL) assay was performed using an Alexa Fluor 488 TUNEL Apoptosis Detection kit (Yeasen, Shanghai, China) according to the manufacturer's instructions. For double staining of TUNEL and CD31, cryosections were fixed in 4% paraformaldehyde for 15 min and then blocked by 5% bull serum albumin for 1 h. The sections were incubated in CD31 (1:200, Santa Cruz, Dallas, TX, USA; sc-376764) antibody solutions overnight at 4 °C, subsequently incubated in equilibration buffer and working strength TdT enzyme at 37 °C for 1 h. The sections were then incubated with Alexa Fluor 594 conjugated secondary antibody (1:400, Invitrogen, Waltham, MA, USA; A32744) and Alexa Fluor 488–12-dUTP Labeling Mix at room temperature for 1 h before imaging. Nuclei were stained with 4′,6-diamidino-2-phenylindole (DAPI). The percentage of endothelial cell apoptotic nuclei was calculated by counting the total number of TUNEL positive nuclei divided by the total number of DAPI stained nuclei on vascular wall (CD31 positive) in 6 fields for each animal at 40 × objective. Image acquisition and quantification was performed by a researcher blinded to the experimental design.

Assays for intracellular reactive oxygen species (ROS) and mitochondrial membrane potential

Flow cytometric analysis was performed on a BD FACScan flow cytometer (FACS Aria II, BD Biosciences, San Jose, CA, USA) with 10,000 events per sample as described. Briefly, at the end of the culture period, the explants were washed once and loaded with 2′7′-dichlorodihydrofluorescein diacetate (H2DCFDA, 10 µM) or 5,5′,6,6′-tetrachloro-1,1′,3,3′-tetraethylbenzimidazolylcarbocyanine iodide (JC-1, 50 nM, Enzo Life Sciences, Farmingdale, NY, USA) at 37 °C in a humidified atmosphere of 95% air and 5% CO_2. After 30 min of incubation, the extracellular H2DCFDA and JC-1 were washed away with hank's balanced salt solution and immediately determined by a FACScan flow cytometer or confocal microscope (Leica, Wetzlar, Germany).

Immunofluorescence assay

The heart cryosections and the coverslips seeded with CMECs were immunofluorescence stained following a routine procedure. The cryosections were fixed with 4% paraformaldehyde for 15 min and then blocked with 5% bull serum albumin for 1 h at room temperature. Slides were incubated overnight at 4 °C with primary antibodies against CD31 (1:200, Santa Cruz; sc-376764), Ve-cadherin (1:200, Santa Cruz; sc-9989), alpha-smooth muscle actin (α-SMA, 1:200, Santa Cruz; sc-53142), von Willebrand Factor (vWF, 1:200, Santa Cruz; sc-365712), transcription factor EB (TFEB, 1:500, Proteintech, Wuhan, China; 13372-1-AP), LC3B (1:200, Abcam, Cambridge, UK; ab192890) and p62 (1:200, Proteintech; 18420-1-AP). After rinsing with phosphate buffer saline, slides were incubated with fluorescence conjugated secondary antibodies for 1 h at room temperature. Slides were photographed using a confocal microscope. Nuclei were stained with DAPI. The percentage of TFEB nuclear translocation in endothelial cells in vivo was calculated by counting the total number of TFEB positive nuclei divided by the total number of DAPI stained nuclei on vascular wall (CD31 positive) in 6 fields for each animal at 40 × objective. The percentage of TFEB nuclear translocation in vitro was calculated in 6 fields for each coverslip at 40 × objective. The microvascular density and integrity were calculated as the area (μm^2) of CD31 and Ve-cadherin puncta within each field, respectively, at least 6 fields for each rat at 40 × objective were quantified. The threshold was set. The α-SMA positive signal was quantified as the same

way. The quantification of fluorescence intensity of LC3B and p62 puncta on vascular endothelium (CD31 positive) within each field was processed by Image J. For each rat, at least 6 fields at 40 × objective were counted. All images were acquired and processed by a researcher blinded to the experimental design.

Assay for autophagic flux using tandem RFP-GFP-LC3B

The autophagic flux in CMECs was assayed using the Premo Autophagy Tandem Sensor Red Fluorescent Protein (RFP)-Green Fluorescent Protein (GFP)-LC3B kit (Invitrogen) following the manufacturer's instructions. 10^4 cells grown on coverslips were incubated with 6 ml of BacMam reagents containing tandem RFP-GFP-LC3B DNA overnight (16 h) and then treated as indicated. Cells were washed and bathed in phosphate buffer saline and visualized through sequential scanning on a confocal microscope.

Western blot analysis

The primary cultured rat CMECs were collected and used to prepare whole cell lysates with radio immunoprecipitation assay buffer supplemented with protease inhibitor cocktail (Roche, Basel, Switzerland). Nuclear and cytoplasmic proteins were extracted from primary rat CMECs cultures using a nuclear and cytoplasmic protein extraction kit (Beyotime, Jiangsu, China). Total proteins (30 μg) were separated by 10% sodium dodecyl sulfate polyacrylamide gel electrophoresis and then transferred onto nitrocellulose membranes. The blots were blocked with 5% fat free milk and incubated overnight at 4 °C with the primary antibodies. Subsequently, the membranes were washed thrice, and then incubated with corresponding horseradish peroxides conjugated secondary antibodies for 1 h at room temperature. Immunoreactive bands were visualized using an enhanced chemiluminescence reagent (Thermo Scientific) and quantified by a Gel-Pro Analyzer (Media Cybernetics, Silver Spring, MD, USA). Primary antibodies against the following proteins were used in the present study: Bax (1:2000; Abcam; ab32503), β-tubulin (1:2000; Abcam; ab6046), Active caspase 3 (1:2000; Abcam; ab32042), Bcl-xL (1:2000; Abcam; ab32370), LC3B (1:1000; Santa Cruz; sc-398822), p62 (1:1500; Santa Cruz; sc-55603), Lysosomal Associated Membrane Protein 1 (LAMP1 1:1000; Santa Cruz; sc-20011), Lysosomal Associated Membrane Protein 2 (LAMP2 1:1000; Santa Cruz; sc-20004), glyceraldehyde-3-phosphate dehydrogenase (GAPDH 1:1000; Abcam; ab8425), Cathepsin B (CTSB 1:1000; Santa Cruz; sc-365558), TFEB (1:1000; Proteintech; 13372-1-AP), lamin A (1:10,000; Abcam; ab8980).

siRNA transfection

For knockdown of TFEB, cells were transfected with TFEB small interfering RNA (siRNA) (Invitrogen) or scramble siRNA using Lipofectamine™ RNAiMAX reagent (Invitrogen). After 24–48 h, siRNA transfected cells were assayed by immunoblotting.

Statistical analysis

All data are presented as the mean ± standard error of the mean. Data were assessed using unpaired Student's *t* test or One-way analysis of variance followed by Student–Newman–Keuls post hoc tests. All results were considered statistically significant if the two-tailed *P* values were less than 0.05. Statistical analysis was performed with SPSS 18.0 (IBM, Armonk, NY, USA).

Result

NAD^+ infusion enhances microvascular density and integrity and reduces no-reflow areas and infarct size in I/R hearts

We first explored whether NAD^+ affected coronary microvascular density and integrity during I/R in the myocardial infarct regions when infusion right before ischemia. The microvascular density and integrity were significantly decreased in the hearts of rats subjected to I/R as indicated by the decreased positive signals of CD31 and Ve-cadherin, respectively, which was prevented by NAD^+ administration (Fig. 1a, b). The α-SMA positive signal was not affected by I/R insult as well as NAD^+ administration (Fig. 1a, b). We further evaluated the regional microvascular perfusion with thioflavin-S staining (thioflavin positive areas, i.e. green and light blue stained areas). Massive no-reflow areas (thioflavin negative areas, i.e. tawny stained areas) were found in myocardial sections of rats subjected to I/R, and NAD^+ administration significantly attenuated the no-reflow areas (Fig. 1c, e). We also observed obvious protective effects of NAD^+ on infarct formation, as indicated by TTC staining (Fig. 1d, e). We further investigated whether NAD^+ also protected coronary microvascular density and integrity and reduced no-reflow areas and infarct size during I/R when given first at reperfusion. NAD^+ significantly prevented the decline of positive signals in CD31 and Ve-cadherin that induced by I/R injury (Fig. 2a, b). NAD^+ also reduced the myocardial no-reflow areas and infarct size even given first at reperfusion (Fig. 2c–e).

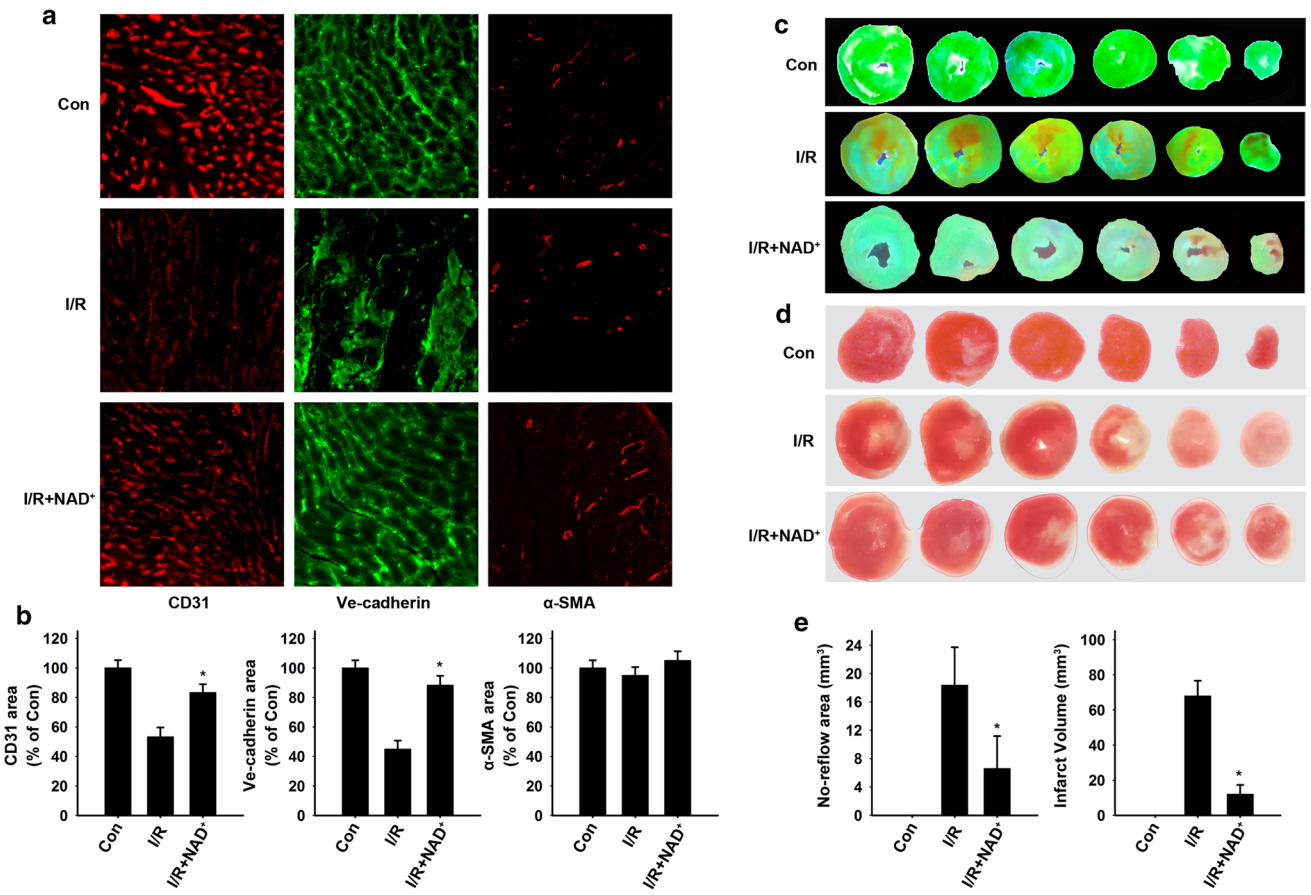

Fig. 1 NAD^+ infusion enhances microvascular density and integrity and reduces no-reflow areas and infarct size in ischemia/reperfusion (I/R) hearts. **a** Representative immunofluorescence images of CD31 (red), Ve-cadherin (green), and α-SMA (red) in rats. Rats were given either saline or NAD^+ (20 mg/kg, 100 mM) and subsequently underwent myocardial I/R. 24 h after the reperfusion, rats were sacrificed and microvascular density, integrity, no-reflow areas, and infarct size in rat hearts were evaluated. **b** Quantification of the area of CD31 (red), Ve-cadherin (green), and α-SMA (red) puncta on myocardial sections of rats, NAD^+ significantly preserved the decline of positive signals of CD31 and Ve-cadherin that induced by I/R injury, NAD^+ seems have little effects on α-SMA positive signal, neither the I/R treatment. $n = 6$ rats per group, $^*P < 0.05$ vs. I/R group. **c** Representative thioflavin-S stained heart sections from the rats that were treated with either saline or 20 mg/kg NAD^+ and subsequently underwent myocardial I/R. 24 h after the I/R, the heart sections were obtained for thioflavin-S staining (thioflavin positive areas, i.e. green and light blue stained areas). **d** Representative TTC stained heart sections from the rats that were treated with either saline or 20 mg/kg NAD^+ and subsequently underwent myocardial I/R. 24 h after the I/R, the heart sections were obtained for TTC staining. **e** Quantifications of the myocardial no-reflow areas (thioflavin negative areas, i.e. tawny stained areas) and infarct size (TTC negative areas, i.e. pale areas). NAD^+ significantly reduced the myocardial no-reflow areas and infarct size. $n = 6$–10 rats per group, $^*P < 0.05$ vs. I/R group

Successful isolation of primary CMECs

Most isolated primary cells were found to have a spindle or cobblestone like morphology at 5–15 days after cell seeding. Further, most isolated primary cells from rat hearts were positively stained by two endothelial cell markers (CD31 and vWF) and co-stained with DAPI, confirming their status as CMECs (Fig. 3a).

NAD^+ attenuates HR-induced CMECs apoptosis changes in vitro

We studied the effects of three dosages of NAD^+ (0 mM, 1 mM, 5 mM, and 10 mM) on HR injury of CMECs, showing that NAD^+ dose-dependently increased the survival of CMECs after HR insult (Fig. 3b). NAD^+ administration also significantly abrogated the HR-induced increase in

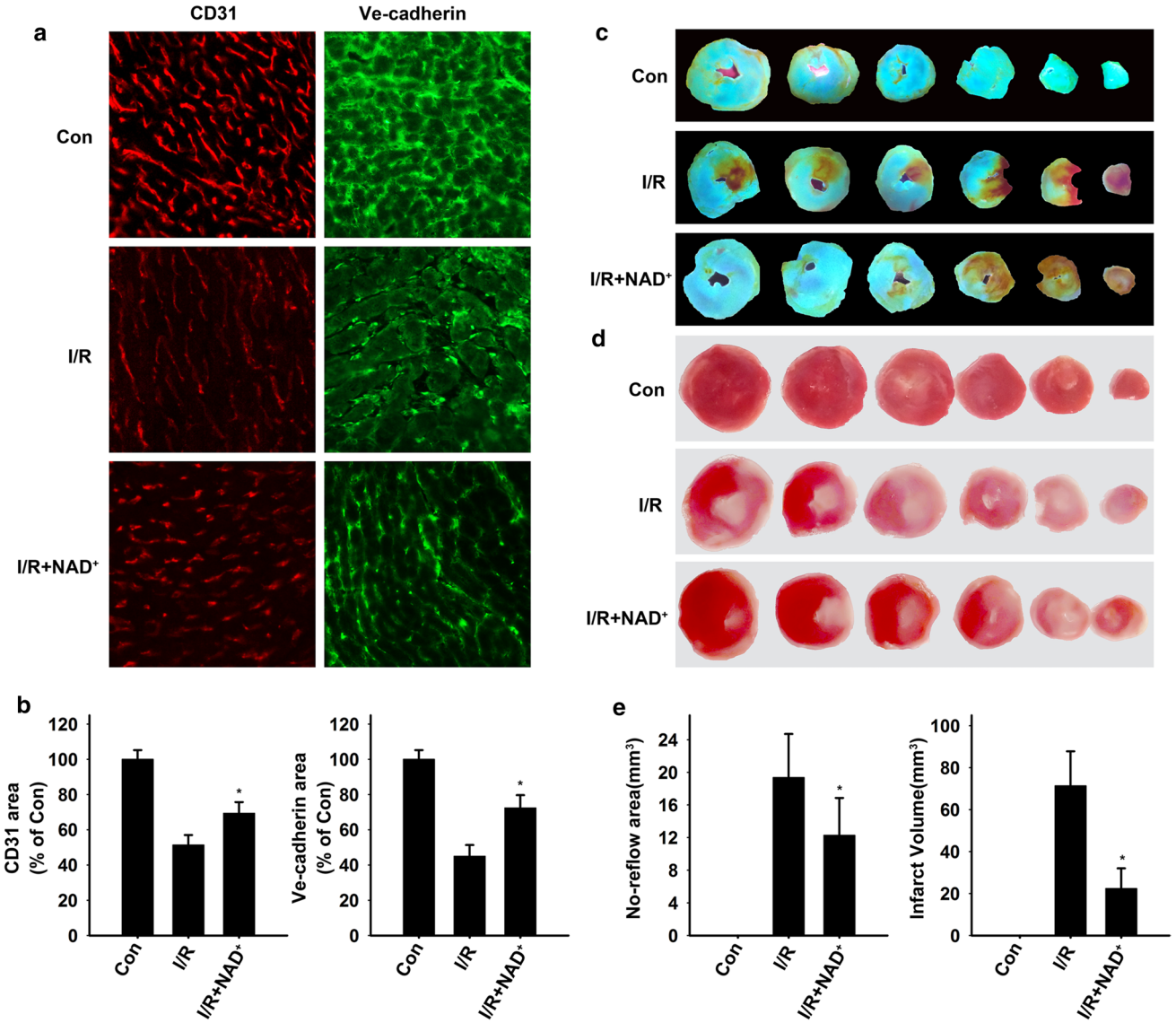

Fig. 2 NAD^+ preserves microvascular density and integrity and reduces no-reflow areas and infarct size in ischemia/reperfusion (I/R) hearts even given first at reperfusion. **a** Rats were given either saline or NAD^+ (20 mg/kg, 100 mM) immediately at reperfusion after 1.5 h of ischemia. 24 h after the reperfusion, the rats were sacrificed and the microvascular density, integrity, no-reflow areas, and infarct size were determined. Representative immunofluorescence images of CD31 (red) and Ve-cadherin (green). **b** Quantification of the area of CD31 and Ve-cadherin puncta on myocardial sections of rats, NAD^+ significantly prevented the decline of positive signals in CD31 and Ve-cadherin that induced by I/R injury. $^*P < 0.05$ vs. I/R group. **c** Representative thioflavin-S stained heart sections. **d** Representative TTC stained heart sections. **e** Quantifications of the myocardial no-reflow areas (thioflavin negative areas, i.e. tawny stained areas) and infarct size (TTC negative areas, i.e. pale areas). NAD^+ reduced the myocardial no-reflow areas and infarct size even given first at reperfusion. $n = 6$–10 rats per group, $^*P < 0.05$ vs. I/R group

Bax and active caspase 3 protein levels in the CMECs subjected to HR. Bcl-xL is a pro-survival protein. We found that NAD^+ administration significantly attenuated the HR-induced decrease in Bcl-xL protein levels in CMECs (Fig. 3c, d). NAD^+ significantly decreased the percentage of cells in apoptosis (Annexin V +), as showed in a FACS-based Annexin V/7-AAD assay (Fig. 3e, f).

Impaired autophagic flux in association with CMECs death after HR

First, we tested the hypothesis that impaired autophagic flux causes CMECs death. Experimental inhibition of autophagosome processing with CQ increased cell death in both the basal state and under rapamycin stimulated autophagy

conditions, as assessed by the LDH assay (Fig. 4a). We further investigated the mechanism of cell death with impaired autophagic flux induced by CQ. In CMECs, CQ induced autophagosome accumulation and led to increased ROS generation with decrease of mitochondrial membrane potential, causing mitochondrial permeabilization and activating apoptosis and/or necrosis. Furthermore, CQ induced ROS generation was found to persist after treatment with cyclosporine A (CSA), an inhibitor of mitochondrial permeability transition pores, thereby implying that ROS generation occurs upstream of mitochondrial permeabilization (Fig. 4b–d). Pretreatment with CSA significantly attenuated CQ induced cell death (Fig. 4e). We next investigated the status of autophagic flux in CMECs after HR by determining the abundance of autophagic proteins in CMECs that insulted by in vitro HR. We found that HR induced the cumulative abundance of LC3B and p62, compared with control cells, as assessed by western blot assay and immunofluorescent staining (Fig. 5a, b). We also determined whether HR induced impairment in autophagosome processing is sufficient to induce cell death. Autophagosome accumulation with HR was associated with ROS generation (Fig. 5d, e) and mitochondrial permeabilization (Fig. 5d, f), although mitochondrial permeabilization was blocked with CSA treatment (Fig. 5d, f), ROS generation persisted (Fig. 5d, e), indicating that ROS generation is upstream of mitochondrial permeabilization, analogous to the observations of CQ induced ROS generation (Fig. 4b–d). Accordingly, CSA attenuated HR-induced cell death (Fig. 5g), mirroring the observations with CQ induced cell death (Fig. 4e). In addition, inhibition of autophagic flux with CQ did not affect the cell death ratio that induced by HR injury (Fig. 5c).

NAD^+ restores the impaired autophagic flux caused by HR in CMECs

Restoring autophagic flux is an emerging concept for cell protection [12, 36]. The influence of NAD^+ on autophagic flux in CMECs was investigated via several approaches. First, we found that NAD^+ weakened the GFP fluorescence in CMECs, as evidenced by Premo Autophagy Tandem Sensor RFP-GFP-LC3B assay [40] (Fig. 6a). Second, we found that NAD^+ alleviated the HR-induced accumulation of LC3B and p62 proteins levels (Fig. 6b, c). Third, we observed that CQ markedly blocked the effects of NAD^+ on the GFP fluorescence in cells (Fig. 6a); likewise, CQ blocked the effects of NAD^+ on the decrease in LC3B and p62 protein levels, as western blot assays indicated (Fig. 6b, c). Fourth, to test the hypothesis that restoring the impaired autophagosome processing by NAD^+ alleviated CMECs death after HR, we found that NAD^+ significantly alleviated the cell death of CMECs insulted by HR injury, and blocking autophagic flux by CQ blunted the protective effect of NAD^+ (Fig. 6d).

NAD^+ restores autophagic flux associated with TFEB activation and the amelioration of lysosomal autophagy function in vitro

To investigate the exact role of NAD^+ on autophagic flux after HR, we evaluated the status of TFEB in CMECs after HR insulted. Under current HR conditions, we failed to find TFEB nuclear translocation. But we observed increased TFEB translocation from the lysosomes to the nuclei in CMECs upon NAD^+ administration (Fig. 7a–c). TFEB has been demonstrated to be a crucial regulator of lysosomal autophagy [29, 33]. To further determine whether the activation of TFEB induced by NAD^+ makes a difference on lysosomal function, we also used siRNA to downregulate TFEB to confirm it from another direction. We examined the expression of LAMP1, which closely tracks lysosome numbers, and LAMP2, which is a crucial determinant of autophagosome lysosome fusion [10]. We found that HR induced a decline in the level of LAMP2, compared with control cells, as assessed by western blot assay, and this was significantly attenuated by NAD^+ administration (Fig. 7d, e). We also evaluated lysosomal function by determining the abundance of the proenzyme and activated forms of CTSB. By detecting the protein abundance of CTSB, an important lysosomal protease, with a western blot assay, we found that the abundance of activated forms of CTSB was significantly decreased in HR-treated cells, and this was significantly attenuated by NAD^+ administration (Fig. 7d, e). On the other hand, the data showed that downregulation of TFEB in CMECs after HR significantly abolished the protection of NAD^+ on autophagy lysosomal function as evidenced by accumulated autophagosomes, LC3B and p62 proteins (Fig. 7d, e), and suppressed lysosomal function as assessed by decreased expression of the lysosomal markers LAMP1, LAMP2 and CTSB (Fig. 7d, e). Knockdown of TFEB also markedly exacerbated the HR insult, as indicated by decreases of the intracellular LDH level (Fig. 7f). Consequently, these observations suggested that NAD^+ induced activation of TFEB significantly rescued the autophagy lysosomal dysfunction and CMECs injury induced by HR.

NAD^+ restores autophagic flux and reduces coronary endothelial cell death after I/R in vivo

We first verified whether NAD^+ restored the impaired autophagic flux through TFEB mediated improvement in lysosomal autophagy function after I/R in vivo by measuring the levels of autophagic markers LC3B, p62 and TFEB in vascular endothelium in vivo, as well as using CQ to downregulate lysosomal autophagy function to further confirm it.

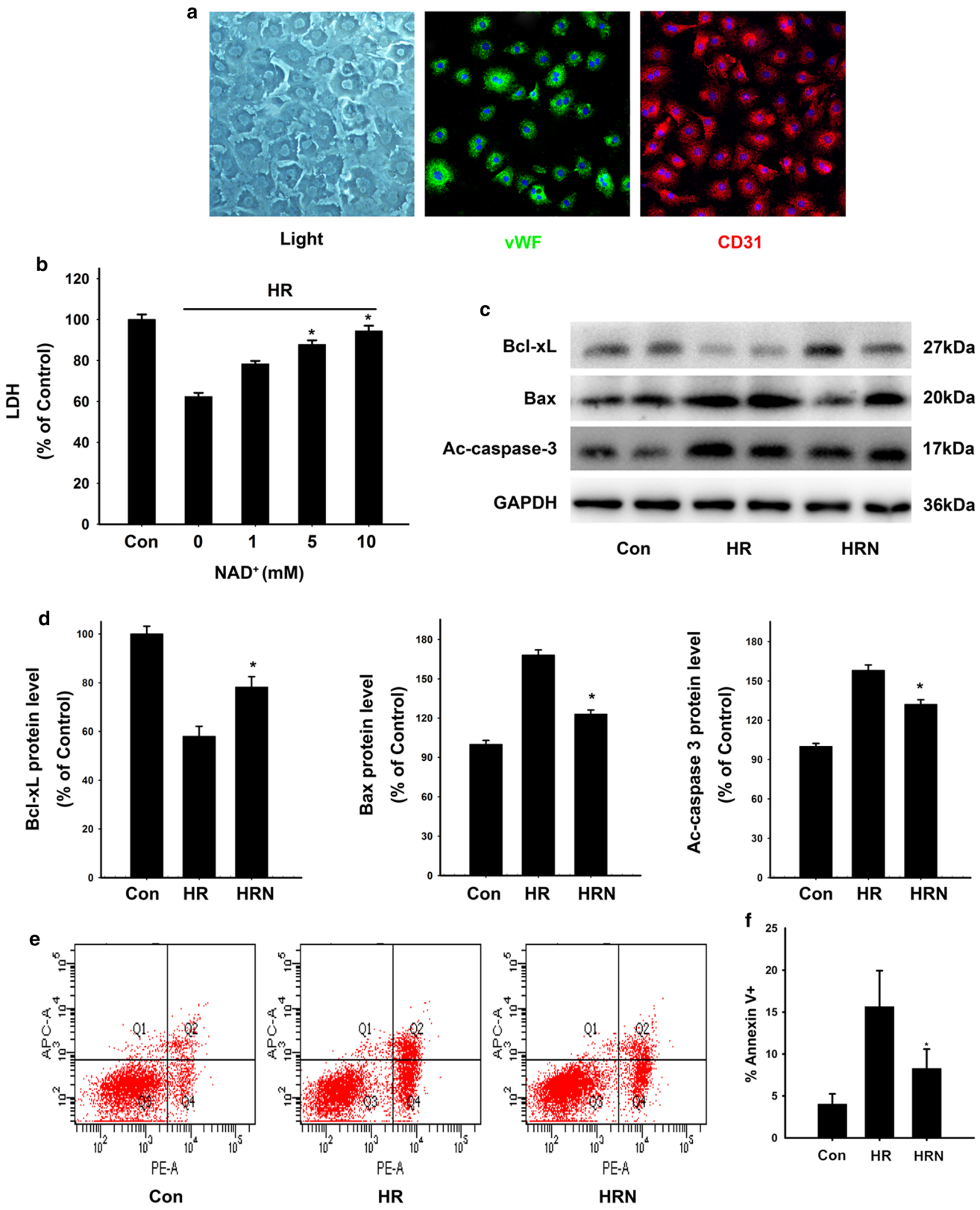

Immunofluorescence images showed markedly higher p62 and LC3B fluorescence intensity on vascular wall in the damaged hearts as compared with the controls, and NAD^+ reduced the accumulated p62 and LC3B levels. Blocking lysosomal autophagy function by CQ blunted the effect of NAD^+ on those autophagic markers (Fig. 8a, b), which was

◂**Fig. 3** NAD^+ attenuates hypoxia/reoxygenation (HR) induced coronary microvascular endothelial cells (CMECs) apoptosis change. **a** The most isolated primary cells were found to have a spindle or cobblestone like morphology at 5–15 days after cell seeding. Representative immunofluorescence images showed that the most isolated primary cells from rat heart were positively stained by two endothelial cell markers (CD31, red and vWF, green) and co-stained with DAPI (blue), confirming their status as CMECs. **b** The NAD^+ administration produced dose dependent protection against HR injury: Both 5 mM and 10 mM NAD^+ significantly increased the intracellular LDH level. $n=5$–9 per group, $^*P<0.05$ vs. HR. **c** Western blots for Bax, active caspase 3 and Bcl-xL in rat CMECs. CMECs were treated with phosphate buffer saline or 5 mM NAD^+ then underwent HR. NAD^+ administration significantly decreased the protein level of Bax, active caspase 3, and increased the protein level of Bcl-xL. **d** Quantifications of protein level of Bax, active caspase 3 and Bcl-xL after treatment with indicated treatments. $n=5$ per group, $^*P<0.05$ vs. HR. **e** Representative images of flow cytometric based Annexin V/7-AAD assay in CMECs. NAD^+ significantly decreased the percentage of the cells in apoptosis (Annexin V+). **f** Quantifications of the percentage of Annexin V+cells. NAD^+ significantly decreased the percentage of cells in apoptosis (Annexin V+). $n=5$ per group, $^*P<0.05$ vs. HR

consistent with the in vitro data. In addition, we found that the accumulated p62 and LC3B signals seemed predominant in the vasculature as compared to the myocardium (Fig. 8a, b).We further determined whether NAD^+ plays a role in TFEB activation in vivo by evaluating the status of TFEB on vascular wall. We found that TFEB failed to translocate to the nuclei after I/R insult but observed increased TFEB translocation from the lysosomes to the nuclei in endothelial cells upon NAD^+ administration (Fig. 8c). To test the hypothesis that restoring the impaired autophagosome processing by NAD^+ alleviated endothelial cell injury after I/R in vivo, we performed a TUNEL and CD31 colocalization assay and found that NAD^+ significantly alleviated the positive TUNEL signal on the vascular wall induced by I/R injury. Furthermore, we used CQ to downregulate the lysosomal function in vivo. CQ significantly abrogated the NAD^+ enhanced lysosomal autophagy function, as evidenced by accumulated fluorescence signal of LC3B and p62 on vascular wall (Fig. 8a, b). CQ also markedly aggravated the apoptosis of CMECs, as indicated by the decreased fluorescence signal of CD31 and increased TUNEL positive signal on vascular wall (Fig. 8d). In addition, CQ was not found to affect TFEB status, indicating that the target of CQ is downstream of TFEB (Fig. 8c).

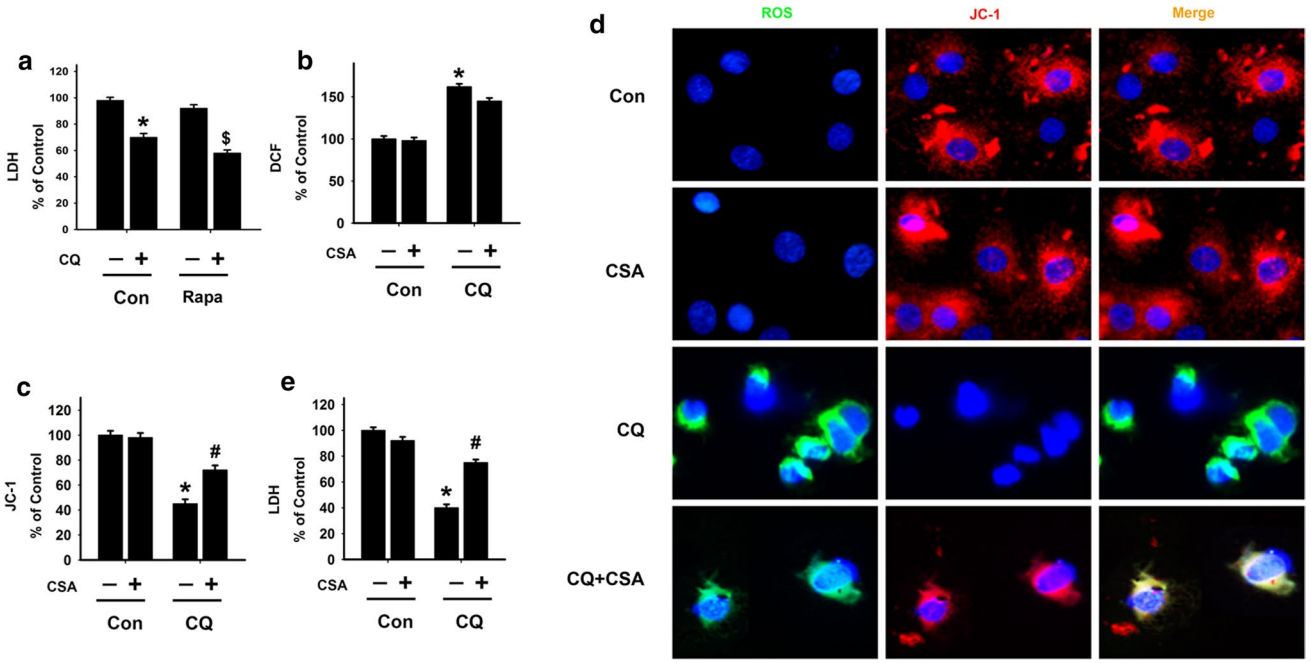

Fig. 4 Impaired autophagic flux is associated with cell death. **a** Intracellular LDH level in coronary microvascular endothelial cells (CMECs) treated with rapamycin (Rapa, 5 μM for 24 h) or vehicle control (Con) in the absence or presence of chloroquine (CQ, 10 μM for 24 h). $n=6$ per group, $^*P<0.05$ vs. Con, $^{\$}P<0.05$ vs. Rapa treatment. **b** Flow cytometric analysis of CMECs treated with CQ (10 μM for 24 h) or Con in the absence or presence of cyclosporine A (CSA, 20 μM) and quantification of mean fluorescence for DCF for reactive oxygen species (ROS), $n=5$ per group, $^*P<0.05$ vs. Con. **c** Flow cytometric analysis of CMECs treated with CQ (10 μM for 24 h) or Con in the absence or presence of CSA (20 μM) and quantification of mean fluorescence for JC-1. $n=5$ per group, $^*P<0.05$ vs. Con, $^{\#}P<0.05$ vs. CQ treatment. **d** Representative images of CMECs loaded with the ROS indicator H2DCFDA (green) and JC-1 (red) after treated with Con or CQ (10 μM) in the presence or absence of CSA (20 μM). **e** Intracellular LDH level in CMECs treated with CQ (10 μM for 24 h) or Con in the absence or presence of CSA (20 μM), $n=6$ per group, $^*P<0.05$ vs. Con, $^{\#}P<0.05$ vs. CQ treatment

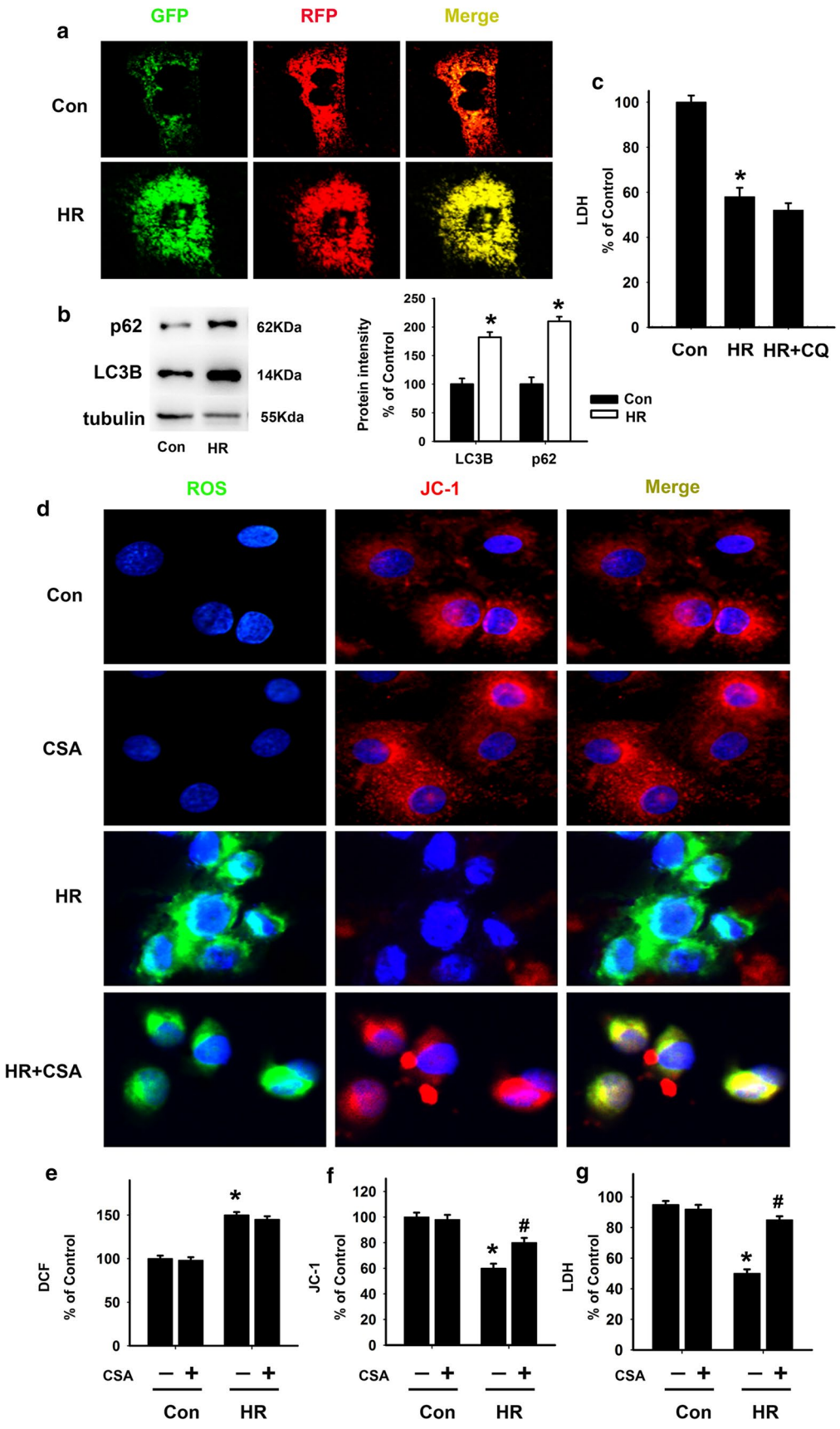
a
GFP
RFP
Merge
Con
HR
b
p62
LC3B
tubulin
62KDa
14KDa
55Kda
Con
HR
Protein intensity
% of Control
LC3B
p62
Con
HR
c
LDH
% of Control
Con
HR
HR+CQ
d
ROS
JC-1
Merge
Con
CSA
HR
HR+CSA
e
DCF
% of Control
CSA
Con
HR
f
JC-1
% of Control
CSA
Con
HR
g
LDH
% of Control
CSA
Con
HR

◂**Fig. 5** Autophagic flux in coronary microvascular endothelial cells (CMECs) is impaired after hypoxia/reoxygenation (HR). **a** Representative immunofluorescence images of rat CMECs expressing RFP-GFP–LC3B and treated with HR or vehicle control (Con) for 24 h. **b** Western blot analysis of LC3B and p62 in CMECs treated with HR and Con for 24 h. Corresponding densitometric analysis of LC3B and p62 bands with respect to each tubulin, $n=5$ per group, $^{*}P<0.05$ vs. Con. **c** Intracellular LDH level in CMECs treated with Con, HR and HR plus chloroquine (CQ, 10 μM) treatment for 24 h. $^{*}P<0.05$ vs. Con. **d** Representative images of CMECs loaded with the reactive oxygen species (ROS) indicator H2DCFDA (green) and JC-1 (red) after treated with HR and Con in the presence or absence of cyclosporine A (CSA, 20 μM). **e** Flow cytometric analysis of CMECs with quantification of mean fluorescence for ROS. $n=5$ per group, $^{*}P<0.05$ vs. Con. **f** Flow cytometric analysis of CMECs with quantification of mean fluorescence for JC-1. $n=5$ per group, $^{*}P<0.05$ vs. Con, $^{\#}P<0.05$ vs. HR. **g** Intracellular LDH level in CMECs treated with HR (24 h) or Con in the presence or absence of CSA (10 μM for 24 h), $n=5$ per group, $^{*}P<0.05$ vs. Con, $^{\#}P<0.05$ vs. HR

Discussion

The present study first demonstrated that NAD^+ infusion preserved the coronary microvascular density and integrity, reduced no-reflow areas and infarct size, and rescued CMECs injury in rat hearts insulted by I/R injury. Such microvasculature protection was at least in part associated with NAD^+ induced TFEB mediated lysosomal autophagy function in CMECs after I/R insult.

Acute myocardial infarction is commonly complicated with coronary microvascular damage, with a high incidence of 50–70% [6]. Although interventional therapy can effectively provide blood reperfusion, successful myocardial perfusion may remain incomplete due to microvascular damage [31]. The coronary circulation is not only as a victim of myocardial I/R injury but after restoration of coronary blood flow it is also the target of I/R injury [16]. It has been demonstrated that I/R induces significant structural damage to the capillaries, such as reduced microvascular density and impairment of endothelial integrity [11]. Targeting the endothelial gap junction Ve-cadherin complex and preserving coronary endothelial integrity following acute myocardial I/R have been reported to reduce infarct size [8]. In the current study, we found that NAD^+ treatment significantly preserved endothelial integrity as indicated by a marked increase in Ve-cadherin signals in rat hearts subjected to myocardial I/R. We also observed that NAD^+ prevented the myocardial I/R-induced decrease in microvascular density as indicated by a marked increase in CD31 signals. Further, we investigated whether the beneficial effect of NAD^+ on microvascular structure can translate to improved myocardial blood flow and reduced the final infarct size. We showed that NAD^+ significantly reduced the no-reflow area that induced by I/R injury as evidenced by thioflavin-S staining results, at least at this time point. We also confirmed prominent protective effects of NAD^+ on the infarct formation in current study. It is noteworthy that NAD^+ could also reduce the I/R induced microvascular injury and infarct size even when administered at reperfusion onset (Fig. 2).

We investigated whether the coronary microvascular protection of NAD^+ was due to a direct vasculoprotective effect of NAD^+ or was secondary to myocardial salvage. Since we initially found NAD^+ significantly rescued the loss of Ve-cadherin and CD31 (endothelial cell marker) signals induced by I/R injury, rather than α-SMA (vascular smooth muscle cell maker) signals (Fig. 1a, b), we separated the CMECs from the rat hearts and used an in vitro HR model to simulate the acute myocardial infarction conditions and investigate the role of NAD^+ on endothelial cell I/R injury.

Our studies have provided several lines of in vitro and in vivo evidence suggesting that NAD^+ decreases CMECs HR injury at least partially by decreasing apoptotic changes: (1) NAD^+ treatment led to a marked increase in LDH levels in rat CMECs that were subjected to simulated HR; (2) NAD^+ treatment could significantly increase cell survival by decreasing early stage apoptosis; (3) NAD^+ administration exhibited a notable decrease in active caspase 3 signals induced by HR; (4) NAD^+ profoundly attenuated the HR-induced increase in Bax levels in rat CMECs; (5) NAD^+ prevented the HR-induced decrease in Bcl-xL levels; and (6) NAD^+ significantly alleviated the positive TUNEL signals in CMECs of rat hearts insulted by I/R injury as indicated by the colocalization of CD31 and TUNEL positive signals (Fig. 8d). Together, these data first confirm that NAD^+ can directly exert protective effects on CMECs under HR and I/R conditions.

The possible mechanisms recruited by NAD^+ for protecting human and rat cardiomyocytes and reducing infarct size in I/R have been associated with ischemic preconditioning [37], oxidative stress, mitochondrial permeabilization [19], and cell death [41]. NAD^+ also partially activates the AMP-activated protein kinase, autophagy and SIRT1 pathway involved in endothelial cell aging and neuron I/R injury, respectively [4, 12, 34]. However, the potential mechanism of NAD^+ in I/R related CMECs death remained largely unaddressed. In fact, there may rather be some common pathomechanisms, such as damage by ROS, mitochondrial permeabilization, and cell death, impact on the myocardial and coronary microvascular compartment, rendering them as targets to not only reduce infarct size but also improve coronary blood flow [14, 15, 22]. Recent studies have indicated that mitochondrial function is vital to maintenance of rat coronary microvascular integrity and endothelial viability [21, 42], which was also implied in current study. The underlying regulatory mechanism responsible for mitochondrial permeabilization, ROS production and cell death was multiple and interacting [22]. Several studies have indicated that autophagic flux can serve as an independent mechanism of cell death, or act as a trigger of apoptosis or necrosis [3].

Notably, contemporary studies demonstrate that impaired autophagic flux prevents the clearance of damaged intracellular organelles and proteins, leading to increased ROS generation, which causes mitochondrial permeabilization and activation of cardiomyocyte and neuron apoptosis and/or necrosis in I/R injury [3, 28]. Thus, in current study, we investigated whether the autophagic pathway is recruited by NAD^+ for protecting the I/R related microvascular injury. First, we evaluated the status of autophagic flux and its role in CMECs under HR conditions using several reliable assays such as a tandem RFP-GFP-LC3B assay, JC-1 assay, ROS assay, and LDH assay. We investigated the influence of HR on autophagic flux, ROS generation, mitochondrial permeabilization and CMECs death by comparing the role of the autophagic flux inhibitor CQ. We found that CQ induced impaired autophagic flux and significantly induced cell death. Similarly, we found that HR significantly enhanced GFP signals as well as LC3B and p62 protein levels, implying impaired autophagic flux, and induced CMECs death. Furthermore, HR exacerbated ROS generation, mitochondrial permeabilization and cell death, mirroring the observations with the autophagic flux inhibitor CQ. In addition, CQ did not affect the CMECs death ratio induced by HR injury, as indicated by LDH assay. The above observations led us to conclude that HR and CQ may share a same mechanism that induces CMECs death, such as defective autophagic flux, consistent with a severe defective autophagic flux in cardiomyocytes subjected to I/R injury [28]. Subsequently, we investigated the role of NAD^+ on autophagic flux in vivo and in vitro. Our study indicated that I/R impaired autophagic flux, and NAD^+ could improve the autophagic processing activity of CMECs after I/R injury, as indicated by the downregulation of GFP, LC3B and p62 fluorescence intensity as well as LC3B and p62 protein levels, which was consistent with previous studies of NAD^+ in human heart ischemic preconditioning [37] and human umbilical vein endothelial cells aging [12]. Furthermore, the positive roles of NAD^+ in autophagic processing and cell viability were abrogated under combined treatment with the autophagic

Fig. 7 NAD^+ restores autophagic flux associated with TFEB activation and the amelioration of lysosomal function in vitro. **a** Primary coronary microvascular endothelial cells (CMECs) were transfected with scramble RNA or TFEB siRNA (siTFEB) for 24 h, and then underwent vehicle control (Con), hypoxia/reoxygenation (HR), HR plus NAD^+ treatment (5 mM, HRN) for 24 h. Representative immunofluorescence images depicting TFEB (green) and DAPI (blue). **b** Quantification of TFEB nuclear positive cells. The percentages of TFEB nuclear positive cells versus total cells are indicated. $n=5$ coverslips per group, $^*P<0.05$ vs. HR, $^{\#}P<0.05$ vs. HRN, at least 1000 cells were quantified per group. **c** Immunoblot assays against TFEB protein of total cytoplasmic and nuclear fractions obtained from CMECs with the indicated treatment. **d** Representative immunoblot images of LC3B, p62, LAMP1, LAMP2 and proenzyme and activated forms of Cathepsin B (CTSB). **e** Quantifications of protein level of LC3B, p62, LAMP1, LAMP2 and activated forms of CTSB. $n=5$ per group, $^{\&}P<0.05$ vs. Con, $^*P<0.05$ vs. HR, $^{\#}P<0.05$ vs. HRN. **f** NAD^+ (5 mM) administration produced a protection against HR injury as indicated by significantly increased the intracellular LDH level, but this protection was abolished with knockdown of TFEB. $n=5$–6 per group, $^*P<0.05$ vs. HR, $^{\#}P<0.05$ vs. HRN

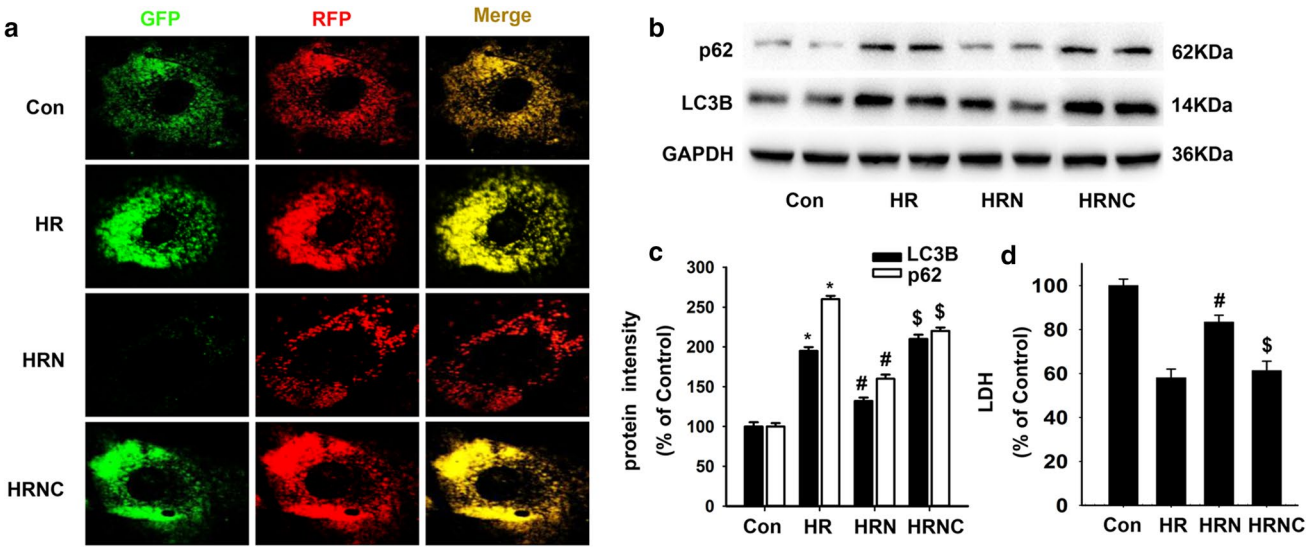

Fig. 6 NAD^+ restores the impaired autophagic flux caused by hypoxia/reoxygenation (HR) in coronary microvascular endothelial cells (CMECs). **a** Cells underwent vehicle control (Con), HR, HR plus NAD^+ treatment (5 mM, HRN) and HR combined with NAD^+ and chloroquine (CQ) co-treatment for 24 h (HRNC). Representative immunofluorescence images of RFP-GFP–LC3B expressing cells. **b** Representative images from immunoblot assays against LC3B, p62 and GAPDH. **c** Quantifications of protein level of LC3B and p62, normalized to the GAPDH, $n=3$–5 per group, $^*P<0.05$ vs. Con, $^{\#}P<0.05$ vs. HR, $^{\$}P<0.05$ vs. HRN. **d** Intracellular LDH level in CMECs that underwent the indicated treatments. $n=5$–6 per group, $^{\#}P<0.05$ vs. HR, $^{\$}P<0.05$ vs. HRN

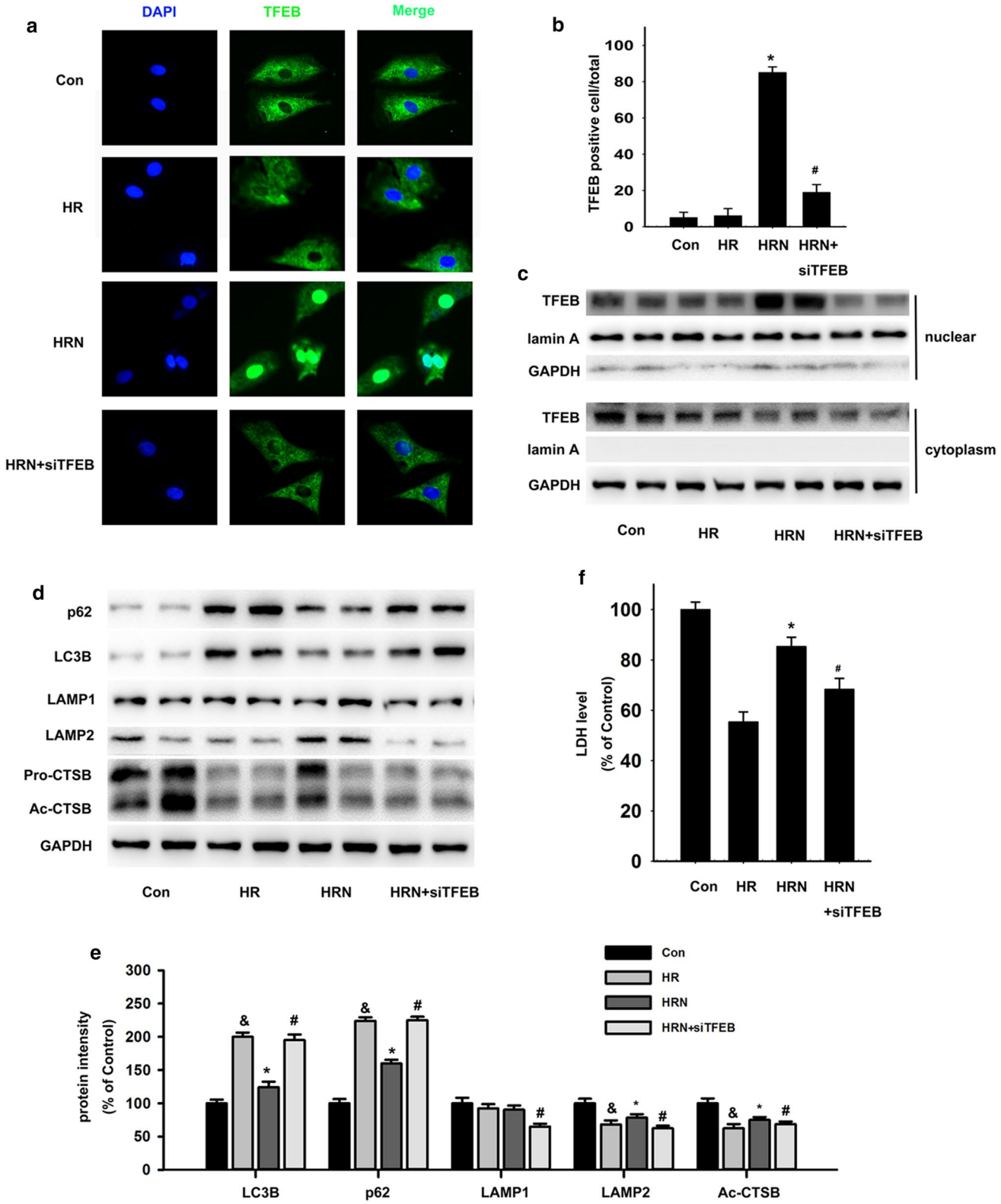

flux inhibitor CQ in I/R-stressed cells. Together, our data indicated that NAD^+ reduced CMECs death via restoring the autophagic flux after I/R.

The underlying mechanism by which autophagic flux is impaired by HR and how it is influenced by NAD^+ were investigated in the current study. Autophagosome clearance can be impaired if lysosome numbers decline or if there is

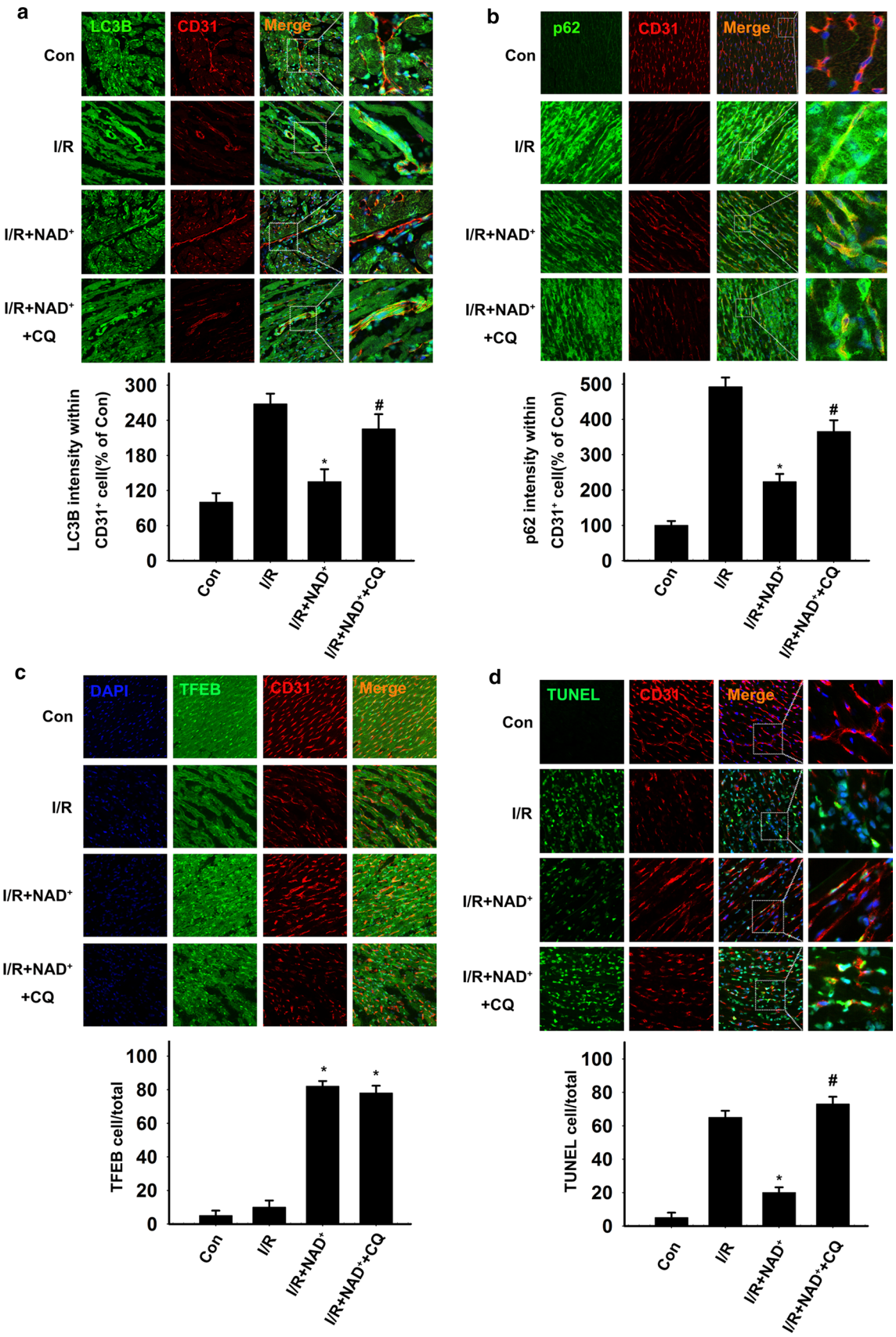
a
LC3B
CD31
Merge
Con
I/R
I/R+NAD+
I/R+NAD+ +CQ
LC3B intensity within CD31+ cell(% of Con)
300
240
180
120
60
0
Con
I/R
I/R+NAD+
I/R+NAD+ +CQ
b
p62
CD31
Merge
p62 intensity within CD31+ cell(% of Con)
500
400
300
200
100
0
c
DAPI
TFEB
CD31
Merge
TFEB cell/total
100
80
60
40
20
0
d
TUNEL
CD31
Merge
TUNEL cell/total

◂**Fig. 8** NAD^+ restores autophagic flux and reduces coronary endothelial cell death after ischemia/reperfusion (I/R) in vivo. **a** Rats were administered with saline or NAD^+ (20 mg/kg, 100 mM) or NAD^+ plus chloroquine (CQ, 10 mg/kg, 100 mM) and subsequently underwent myocardial I/R. 24 h after the reperfusion. High magnification images of rat heart sections stained with antibodies against LC3B (green) and CD31 (red), merged images include DAPI staining (blue). Quantifications of LC3B fluorescence intensity on vascular endothelium ($CD31^+$ cell) in the heart of rats, $n=6$ rats per group, at least 6 fields for each rat at 40× objective were calculated. $^*P<0.05$ vs. I/R, $^{\#}P<0.05$ vs. I/R + NAD^+. **b** High magnification images of rat heart sections stained with antibodies against p62 (green) and CD31 (red), merged images include DAPI staining (blue). Quantifications of p62 fluorescence intensity on vascular endothelium ($CD31^+$ cell) in the heart of rats, $n=6$ rats per group, at least 6 fields for each rat at 40× objective were calculated.$^*P<0.05$ vs. I/R, $^{\#}P<0.05$ vs. I/R + NAD^+. **c** Images of rat heart sections stained with antibodies against TFEB (green) and endothelial cell marker CD31 (red), merged images include DAPI staining (blue). Quantification of CD31 and nuclear TFEB double positive cells, the percentages of double-positive cells versus total CD31 positive cells are indicated. $n=6$ rats per group, at least 6 fields for each rat heart at 40× objective were counted. $^*P<0.05$ vs. I/R. **d** Images of rat heart sections stained with TUNEL (green) and endothelial cell marker CD31 (red), merged images include DAPI staining (blue). Quantification of TUNEL and CD31 double-positive cells, the percentages of double positive cells versus total CD31 positive cells are indicated. $n=6$ rats per group, at least 6 fields for each rat at 40× objective were counted. $^*P<0.05$ vs. I/R, $^{\#}P<0.05$ vs. I/R + NAD^+

a impairment in autophagosome lysosome fusion or lysosomal function in I/R-related diseases, such as stroke and acute myocardial infarction [26, 28]. In our CMECs HR model, we observed that HR blocked autophagosome lysosome fusion, as indicated by the decreased level of LAMP2, a critical determinant of autophagosome lysosome fusion, which was consistent with previous studies in cardiomyocyte I/R injury [1, 28]. Nevertheless, we also found that HR induced the loss of lysosomal degradation activity, with associated downregulation of the activated forms of CTSB. However, NAD^+ treatment restored the impaired lysosomal function induced by HR. How NAD^+ repaired the lysosomal function was unclear so far. Since variation in TFEB translocation is closely associated with changes in lysosomal autophagy function [26], it is reasonable to assume that NAD^+ may influence TFEB nuclear translocation. As expected, the in vitro and in vivo data first showed that NAD^+ significantly activated the TFEB function and exerted beneficial effects on lysosomal autophagy function in CMECs. In further supporting that NAD^+ repaired the lysosomal function is at least partially dependent on TFEB, we used an in vitro TFEB targeted siRNA to downregulate TFEB expression. TFEB knockdown was effective in reversing the NAD^+ alleviated accumulation of autophagosomes and impaired lysosomal function. Moreover, we found that knockdown of TFEB triggered a further loss of CMECs in vitro. Furthermore, we used CQ to downregulate lysosomal function in vivo. The lysosomal autophagy dysfunction induced by CQ significantly abolished the NAD^+ alleviated accumulation of autophagosomes and coronary endothelial cell loss after I/R injury in vivo, suggesting that lysosomal autophagy function is involved in NAD^+ regulated TFEB signaling cascades. Collectively, the present study supports the idea that NAD^+ induced TFEB-mediated activation of lysosomal autophagy function may play a pro-survival role in CMECs after I/R injury.

In summary, the current study has provided the first evidence that exogenous NAD^+ infusion preserved microvascular density and integrity, reduced no-reflow areas and infarct size, and rescued CMECs injury in rat hearts insulted by I/R. We also found that impaired autophagic flux at least partially plays a role in I/R or HR-induced endothelial cell death. Importantly, NAD^+ significantly rescued the impaired autophagic flux and cell death induced by I/R or HR in rat CMECs, which appears to be mediated in part through the action of TFEB mediated lysosomal autophagy. These results identify NAD^+ as a promising target for therapies aimed at coronary microvascular I/R injury.

There are several limitations of our current study. First, the no-reflow phenomenon can be seen within minutes after reperfusion. In this context, protection by activation of TFEB seems too slow for the early phase I/R injury. Second, the no-reflow phenomenon changes dynamically and persists long term after I/R [32]. Reduction of no-reflow areas at one time point does not make sure long term improved myocardial perfusion and prognosis. It requires further robust data with time-course and dose–response relationships to confirm NAD^+ is druggable and translatable for cardioprotection.

Acknowledgements The authors would like to acknowledge the financial support by a National Natural Science Foundation of China (81770420 and 61533016 to X.Q.), a Center of Geriatric Coronary Artery Disease, a Major Research Grant from the Scientific Committee of Shanghai Municipality (16JC1400500 and 16JC1400502 to W.Y.), and a Major Special Program Grant of Shanghai Municipality (2017SHZDZX01 to W.Y.), Research Fund for the Scientific and Technical Project of Huadong Hospital (2019JC024 to Z.Y.J.)

Compliance with ethical standards

Conflict of interest The authors declare that they have no conflict of interest.

References

1. Bhuiyan MS, Pattison JS, Osinska H, James J, Gulick J, McLendon PM, Hill JA, Sadoshima J, Robbins J (2013) Enhanced autophagy ameliorates cardiac proteinopathy. J Clin Invest 12312:5284–5297. https://doi.org/10.1172/jci70877
2. Botker HE, Hausenloy D, Andreadou I, Antonucci S, Boengler K, Davidson SM, Deshwal S, Devaux Y, Di Lisa F, Di Sante M, Efentakis P, Femmino S, Garcia-Dorado D, Giricz Z, Ibanez

B, Iliodromitis E, Kaludercic N, Kleinbongard P, Neuhauser M, Ovize M, Pagliaro P, Rahbek-Schmidt M, Ruiz-Meana M, Schluter KD, Schulz R, Skyschally A, Wilder C, Yellon DM, Ferdinandy P, Heusch G (2018) Practical guidelines for rigor and reproducibility in preclinical and clinical studies on cardioprotection. Basic Res Cardiol 1135:39. https://doi.org/10.1007/s00395-018-0696-8

3. Cui D, Sun D, Wang X, Yi L, Kulikowicz E, Reyes M, Zhu J, Yang ZJ, Jiang W, Koehler RC (2017) Impaired autophagosome clearance contributes to neuronal death in a piglet model of neonatal hypoxic-ischemic encephalopathy. Cell Death Dis 87:e2919. https://doi.org/10.1038/cddis.2017.318
4. Das A, Huang GX, Bonkowski MS, Longchamp A, Li C, Schultz MB, Kim LJ, Osborne B, Joshi S, Lu Y, Trevino-Villarreal JH, Kang MJ, Hung TT, Lee B, Williams EO, Igarashi M, Mitchell JR, Wu LE, Turner N, Arany Z, Guarente L, Sinclair DA (2018) Impairment of an endothelial NAD(+)-H2S signaling network is a reversible cause of vascular aging. Cell 1731:74–89 e20. https://doi.org/10.1016/j.cell.2018.02.008
5. Davidson SM, Ferdinandy P, Andreadou I, Botker HE, Heusch G, Ibanez B, Ovize M, Schulz R, Yellon DM, Hausenloy DJ, Garcia-Dorado D (2019) Multitarget strategies to reduce myocardial ischemia/reperfusion injury: JACC review topic of the week. J Am Coll Cardiol 731:89–99. https://doi.org/10.1016/j.jacc.2018.09.086
6. de Waha S, Patel MR, Granger CB, Ohman EM, Maehara A, Eitel I, Ben-Yehuda O, Jenkins P, Thiele H, Stone GW (2017) Relationship between microvascular obstruction and adverse events following primary percutaneous coronary intervention for ST-segment elevation myocardial infarction: an individual patient data pooled analysis from seven randomized trials. Eur Heart J 3847:3502–3510. https://doi.org/10.1093/eurheartj/ehx414
7. Fan Y, Lu H, Liang W, Garcia-Barrio MT, Guo Y, Zhang J, Zhu T, Hao Y, Zhang J, Chen YE (2018) Endothelial TFEB (transcription factor eb) positively regulates postischemic angiogenesis. Circ Res 1227:945–957. https://doi.org/10.1161/circresaha.118.312672
8. Galaup A, Gomez E, Souktani R, Durand M, Cazes A, Monnot C, Teillon J, Le Jan S, Bouleti C, Briois G, Philippe J, Pons S, Martin V, Assaly R, Bonnin P, Ratajczak P, Janin A, Thurston G, Valenzuela DM, Murphy AJ, Yancopoulos GD, Tissier R, Berdeaux A, Ghaleb B, Germain S (2012) Protection against myocardial infarction and no-reflow through preservation of vascular integrity by angiopoietin-like 4. Circulation 1251:140–149. https://doi.org/10.1161/CIRCULATIONAHA.111.049072
9. Gedik N, Thielmann M, Kottenberg E, Peters J, Jakob H, Heusch G, Kleinbongard P (2014) No evidence for activated autophagy in left ventricular myocardium at early reperfusion with protection by remote ischemic preconditioning in patients undergoing coronary artery bypass grafting. PLoS ONE 95:e96567. https://doi.org/10.1371/journal.pone.0096567
10. Godar RJ, Ma X, Liu H, Murphy JT, Weinheimer CJ, Kovacs A, Crosby SD, Saftig P, Diwan A (2015) Repetitive stimulation of autophagy-lysosome machinery by intermittent fasting preconditions the myocardium to ischemia-reperfusion injury. Autophagy 119:1537–1560. https://doi.org/10.1080/15548627.2015.1063768
11. Granger DN, Kvietys PR (2017) Reperfusion therapy—what's with the obstructed, leaky and broken capillaries? Pathophysiology 244:213–228. https://doi.org/10.1016/j.pathophys.2017.09.003
12. Han X, Tai H, Wang X, Wang Z, Zhou J, Wei X, Ding Y, Gong H, Mo C, Zhang J, Qin J, Ma Y, Huang N, Xiang R, Xiao H (2016) AMPK activation protects cells from oxidative stress-induced senescence via autophagic flux restoration and intracellular NAD(+) elevation. Aging Cell 153:416–427. https://doi.org/10.1111/acel.12446
13. Heusch G, Kleinbongard P, Skyschally A, Levkau B, Schulz R, Erbel R (2012) The coronary circulation in cardioprotection: more than just one confounder. Cardiovasc Res 942:237–245. https://doi.org/10.1093/cvr/cvr271
14. Heusch G (2015) Molecular basis of cardioprotection: signal transduction in ischemic pre-, post-, and remote conditioning. Circ Res 1164:674–699. https://doi.org/10.1161/circresaha.116.305348
15. Heusch G (2016) The coronary circulation as a target of cardioprotection. Circ Res 11810:1643–1658. https://doi.org/10.1161/circresaha.116.308640
16. Heusch G, Gersh BJ (2017) The pathophysiology of acute myocardial infarction and strategies of protection beyond reperfusion: a continual challenge. Eur Heart J 3811:774–784. https://doi.org/10.1093/eurheartj/ehw224
17. Heusch G (2019) Coronary microvascular obstruction: the new frontier in cardioprotection. Basic Res Cardiol 1146:45. https://doi.org/10.1007/s00395-019-0756-8
18. Heusch G, Kleinbongard P, Rassaf T (2019) Cardioprotection beyond infarct size reduction. Circ Res 1245:679–680. https://doi.org/10.1161/circresaha.119.314679
19. Hosseini L, Vafaee MS, Badalzadeh R (2019) Melatonin and nicotinamide mononucleotide attenuate myocardial ischemia/reperfusion injury via modulation of mitochondrial function and hemodynamic parameters in aged rats. J Cardiovasc Pharmacol Ther. https://doi.org/10.1177/1074248419882002
20. Jahania SM, Sengstock D, Vaitkevicius P, Andres A, Ito BR, Gottlieb RA, Mentzer RM Jr (2013) Activation of the homeostatic intracellular repair response during cardiac surgery. J Am Coll Surg 2164:719–726. https://doi.org/10.1016/j.jamcollsurg.2012.12.034**(discussion 726-719)**
21. Kadlec AO, Beyer AM, Ait-Aissa K, Gutterman DD (2016) Mitochondrial signaling in the vascular endothelium: beyond reactive oxygen species. Basic Res Cardiol 1113:26. https://doi.org/10.1007/s00395-016-0546-5
22. Kleinbongard P, Heusch G (2015) Extracellular signalling molecules in the ischaemic/reperfused heart—druggable and translatable for cardioprotection? Br J Pharmacol 1728:2010–2025. https://doi.org/10.1111/bph.12902
23. Lee Y, Kwon I, Jang Y, Song W, Cosio-Lima LM, Roltsch MH (2017) Potential signaling pathways of acute endurance exercise-induced cardiac autophagy and mitophagy and its possible role in cardioprotection. J Physiol Sci 676:639–654. https://doi.org/10.1007/s12576-017-0555-7
24. Li Y, Liang P, Jiang B, Tang Y, Liu X, Liu M, Sun H, Chen C, Hao H, Liu Z, Xiao X (2020) CARD9 promotes autophagy in cardiomyocytes in myocardial ischemia/reperfusion injury via interacting with Rubicon directly. Basic Res Cardiol 1153:29. https://doi.org/10.1007/s00395-020-0790-6
25. Lindsey ML, Bolli R, Canty JM Jr, Du XJ, Frangogiannis NG, Frantz S, Gourdie RG, Holmes JW, Jones SP, Kloner RA, Lefer DJ, Liao R, Murphy E, Ping P, Przyklenk K, Recchia FA, Schwartz Longacre L, Ripplinger CM, Van Eyk JE, Heusch G (2018) Guidelines for experimental models of myocardial ischemia and infarction. Am J Physiol Heart Circ Physiol 3144:H812–H838. https://doi.org/10.1152/ajpheart.00335.2017
26. Liu Y, Xue X, Zhang H, Che X, Luo J, Wang P, Xu J, Xing Z, Yuan L, Liu Y, Fu X, Su D, Sun S, Zhang H, Wu C, Yang J (2018) Neuronal-targeted TFEB rescues dysfunction of the autophagy-lysosomal pathway and alleviates ischemic injury in permanent cerebral ischemia. Autophagy. https://doi.org/10.1080/15548627.2018.1531196
27. Ma X, Liu H, Foyil SR, Godar RJ, Weinheimer CJ, Diwan A (2012) Autophagy is impaired in cardiac ischemia-reperfusion injury. Autophagy 89:1394–1396. https://doi.org/10.4161/auto.21036

28. Ma X, Liu H, Foyil SR, Godar RJ, Weinheimer CJ, Hill JA, Diwan A (2012) Impaired autophagosome clearance contributes to cardiomyocyte death in ischemia/reperfusion injury. Circulation 12525:3170–3181. https://doi.org/10.1161/circulationaha.111.041814
29. Medina DL, Di Paola S, Peluso I, Armani A, De Stefani D, Venditti R, Montefusco S, Scotto-Rosato A, Prezioso C, Forrester A, Settembre C, Wang W, Gao Q, Xu H, Sandri M, Rizzuto R, De Matteis MA, Ballabio A (2015) Lysosomal calcium signalling regulates autophagy through calcineurin and TFEB. Nat Cell Biol 173:288–299. https://doi.org/10.1038/ncb3114
30. Nadtochiy SM, Wang YT, Nehrke K, Munger J, Brookes PS (2018) Cardioprotection by nicotinamide mononucleotide (NMN): Involvement of glycolysis and acidic pH. J Mol Cell Cardiol 121:155–162. https://doi.org/10.1016/j.yjmcc.2018.06.007
31. Niccoli G, Montone RA, Ibanez B, Thiele H, Crea F, Heusch G, Bulluck H, Hausenloy DJ, Berry C, Stiermaier T, Camici PG, Eitel I (2019) Optimized treatment of ST-elevation myocardial infarction. Circ Res 1252:245–258. https://doi.org/10.1161/circresaha.119.315344
32. Reffelmann T, Kloner RA (2002) Microvascular reperfusion injury: rapid expansion of anatomic no reflow during reperfusion in the rabbit. Am J Physiol Heart Circ Physiol 2833:H1099–1107. https://doi.org/10.1152/ajpheart.00270.2002
33. Settembre C, Di Malta C, Polito VA, Garcia Arencibia M, Vetrini F, Erdin S, Erdin SU, Huynh T, Medina D, Colella P, Sardiello M, Rubinsztein DC, Ballabio A (2011) TFEB links autophagy to lysosomal biogenesis. Science 3326036:1429–1433. https://doi.org/10.1126/science.1204592
34. Wang P, Guan YF, Du H, Zhai QW, Su DF, Miao CY (2012) Induction of autophagy contributes to the neuroprotection of nicotinamide phosphoribosyltransferase in cerebral ischemia. Autophagy 81:77–87. https://doi.org/10.4161/auto.8.1.18274
35. Xie M, Kong Y, Tan W, May H, Battiprolu PK, Pedrozo Z, Wang ZV, Morales C, Luo X, Cho G, Jiang N, Jessen ME, Warner JJ, Lavandero S, Gillette TG, Turer AT, Hill JA (2014) Histone deacetylase inhibition blunts ischemia/reperfusion injury by inducing cardiomyocyte autophagy. Circulation 12910:1139–1151. https://doi.org/10.1161/circulationaha.113.002416
36. Xie Y, Jiang D, Xiao J, Fu C, Zhang Z, Ye Z, Zhang X (2018) Ischemic preconditioning attenuates ischemia/reperfusion-induced kidney injury by activating autophagy via the SGK1 signaling pathway. Cell Death Dis 93:338. https://doi.org/10.1038/s41419-018-0358-7
37. Yamamoto T, Byun J, Zhai P, Ikeda Y, Oka S, Sadoshima J (2014) Nicotinamide mononucleotide, an intermediate of NAD+ synthesis, protects the heart from ischemia and reperfusion. PLoS ONE 96:e98972. https://doi.org/10.1371/journal.pone.0098972
38. Zhang DX, Zhang JP, Hu JY, Huang YS (2016) The potential regulatory roles of NAD(+) and its metabolism in autophagy. Metabolism 654:454–462. https://doi.org/10.1016/j.metabol.2015.11.010
39. Zhang H, Ge S, He K, Zhao X, Wu Y, Shao Y, Wu X (2019) FoxO1 inhibits autophagosome-lysosome fusion leading to endothelial autophagic-apoptosis in diabetes. Cardiovasc Res. https://doi.org/10.1093/cvr/cvz014
40. Zhang Y, Xu M, Xia M, Li X, Boini KM, Wang M, Gulbins E, Ratz PH, Li PL (2014) Defective autophagosome trafficking contributes to impaired autophagic flux in coronary arterial myocytes lacking CD38 gene. Cardiovasc Res 1021:68–78. https://doi.org/10.1093/cvr/cvu011
41. Zhang Y, Wang B, Fu X, Guan S, Han W, Zhang J, Gan Q, Fang W, Ying W, Qu X (2016) Exogenous NAD(+) administration significantly protects against myocardial ischemia/reperfusion injury in rat model. Am J Transl Res 88:3342–3350
42. Zhou H, Wang J, Zhu P, Zhu H, Toan S, Hu S, Ren J, Chen Y (2018) NR4A1 aggravates the cardiac microvascular ischemia reperfusion injury through suppressing FUNDC1-mediated mitophagy and promoting Mff-required mitochondrial fission by CK2alpha. Basic Res Cardiol 1134:23. https://doi.org/10.1007/s00395-018-0682-1